Pergamon

Bioorganic & Medicinal Chemistry 8 (2000) 2617–2628

BIOORGANIC & MEDICINAL CHEMISTRY

Comparative Quantitative Structure–Activity Study of Radical Scavengers

Opa Vajragupta,[a,*] Preecha Boonchoong[a] and Yuvadee Wongkrajang[b]

[a]*Department of Pharmaceutical Chemistry, Faculty of Pharmacy, Mahidol University, 447 Sri-Ayudhya Road, Bangkok 10400, Thailand*
[b]*Department of Physiology, Faculty of Pharmacy, Mahidol University, 447 Sri-Ayudhya Road, Bangkok 10400, Thailand*

Received 8 May 2000; accepted 8 July 2000

Abstract—Classic and three-dimensional (3-D) QSAR analyses of 13 radical scavengers (**1**–**13**) were performed to derive two classic, two Apex–3-D and one comparative field analysis (CoMFA) models. Two classical models with predictive cross-validated r^2 (Q^2) over 0.96 indicated that the activity was attributed to the electronic C_{OH} and E_{LUMO}, steric molar refractivity (MR) and lipophilic log *P*. Three-dimensional quantitative structure–activity relationship (3-D–QSAR) studies were performed by 3-D pharmacophore generation (Apex–3-D) and CoMFA techniques. For Apex–3-D studies, two best models with high Q^2 (0.94 and 0.97) were yielded. Structural properties contributing to the activity were not only lipophilic but also the optimum steric property and geometry of side-chain composition. For CoMFA studies, the sp^3 $C(+1)$ probe provided the best Q^2 of 0.79 with steric and electrostatic contributions of 42.3 and 57.7%, respectively. The activity of four new compounds (**14**–**17**) not included in the derivation were predicted with these models. Although the derived models were from limited data, the statistic relation was predictive. The linear correlations between the experimental IC_{50} values and the predicted values from classical and Apex–3-D models were found to be high and significant. The predicted activity of **17** from CoMFA was much lower than the experimental value; this deviation occurred according to the missing of hydrophobic field in standard CoMFA study. In vitro and ex vivo antilipid peroxidation in mouse brain and ESR studies of **14**–**17** were investigated for the radical-scavenging ability. The difference between the in vitro results, antilipid peroxidation and electron spin resonance (ESR) and ex vivo results in coumarin series was found. Thus, other properties for good bioavailability besides log *P* should also be taken into consideration.

Introduction

Free radicals with the major species of reactive oxygen species (ROS) such as superoxide ($O_2^{-\bullet}$), hydroxyl radical ($^{\bullet}OH$), oxide of nitrogen ($NO^{\bullet}$, $NO_2^{\bullet}$), and lipid radicals ($RO^{\bullet}$, $ROO^{\bullet}$, $R^{\bullet}$) are unstable and react readily with other groups or substances in the body, resulting in cell damage and hence human disease.[1–3] Lipids of biological membranes, especially those in the spinal cord and brain containing highly oxidizable polyunsaturated fatty acids, are particularly affected.[4] Moreover, the brain contains considerable amounts of prooxidant transition metal ions and utilizes a lot of oxygen. These properties set the stage for ROS generation and the subsequent acute cellular injury following traumatic brain injury and cerebral ischemia and reperfusion.[5–8] Free radicals are implicated in the aging process and in some diseases including Alzheimer's, Parkinson, ischemic reperfusion injury, arthritis, myocardial infarction, arteriosclerosis and cancer.[9–15]

Because of the impact of these free radicals, many substances have been studied for antiradical properties. α-Tocopherol is the major agent that has been continually developed by adding or changing substituent groups resulting in new antiradical agents such as DL-tocopheryl nicotinate, trolox and its analogues.[16] The shape and structure of the nucleus ring (major ring) containing an hydroxyl group were changed in order to increase electron transfer and improve stability in the human body. For instance, the chroman ring of vitamin E was modified to give benzofuran,[17] amino-coumaran,[18] indole[19] and indan.[20]

In a former study, 13 chroman amides and nicotinyl amides were synthesized by varying both the acid and amine functions of amides. Nine compounds were inhibitors of lipid peroxidation in vitro. It was found that chroman amides had a greater lipid peroxidation inhibitory effect than hydroxynicotinyl amide, whereas nicotinic amides had no effect. It was also reported that

*Corresponding author. Fax: 66-2-247-4696;
e-mail: pyovj@mahidol.ac.th

0968-0896/00/$ - see front matter
PII: S0968-0896(00)00195-4

the inhibition of lipid peroxidation was related to ability to transfer electrons of antiradical agents while lipophilicity was relevant to the capacity of these agents to reach the area where lipid peroxidation occurred.[21]

In this paper, the relationship between the structure/physicochemical properties and lipid peroxidation inhibitory activities of these 13 compounds was studied by both classical quantitative structure–activity relationship (QSAR) and three-dimensional quantitative structure activity relationship (3-D–QSAR) techniques using molecular modeling programs (Table 1). The predictive power of the models derived from QSAR studies was tested on new compounds **14**–**17** (Fig. 1). The ex vivo antilipid peroxidation of these new compounds and their •OH scavenging ability were also evaluated.

Chemistry

The quantitative relation between activity and structure/physicochemical properties was determined using classical and 3-D procedures. The classical QSAR and 3-D–QSAR models were generated from the initial data set of 13 previously synthesized compounds and trolox. In classical QSAR studies, the in vitro percent inhibition of lipid peroxidation represented the activity (dependent variable) and the independent variables were steric, electronic and hydrophobic descriptors. For 3-D–QSAR studies, pharmacophore generation (Apex–3-D module in Insight II release 95.0)[22] and comparative field analysis (CoMFA, Sybyl 6.3)[23] were the techniques used to generate the QSAR models. Four new compounds, coumarin amides (**14**–**16**), and one related chroman amide **17**, were prepared in order to test the predictive power of the derived QSAR models. They were synthesized by using *N,N′*-carbonyldiimidazole (CDI) as coupling agent. The physical properties of the compounds synthesized are listed in Table 2.

Electron spin resonance (ESR) studies of these four compounds to trap •OH were evaluated using $H_2O_2/CuSO_4$ to generate •OH and α-phenyl-*N*-*tert*-butylnitrone (PBN) as spin trap in order to determine the scavenging ability of synthesized compounds against hydroxy radical. Chroman derivatives reacted with hydroxyl radical yielding ESR signals of chromanoxyl radicals, whereas ESR signal was not found from all coumarin amides under

Table 1. Descriptors used in the QSAR study

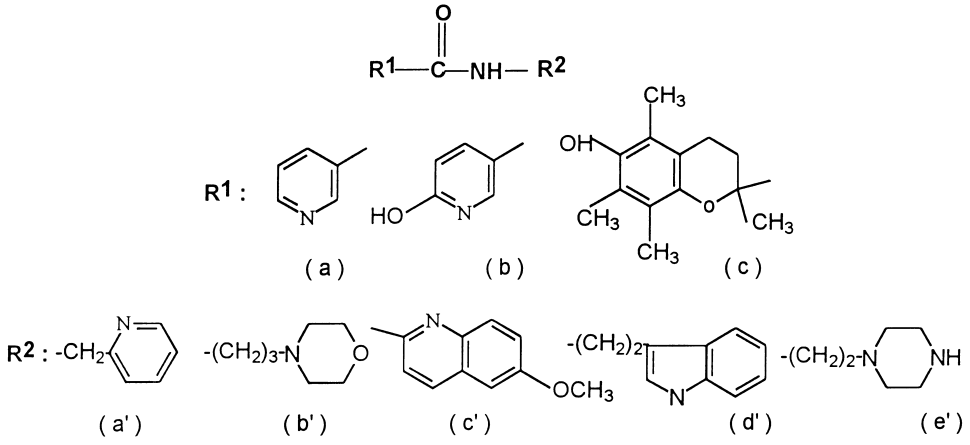

Compounds	R^1	R^2	%[a]	MR[b]	Lipophilicity			OH-indicator	Charge C_{OH}	Molecular orbital energy (eV)	
					H[c]	CLOGP[d]	Log *P*[e]			E_{LUMO}	E_{HOMO}
1	a	a′	0.00	59.462	0.677	0.379	0.66	0	0	−0.4027	−9.9176
2	a	b′	0.00	69.225	−0.302	0.075	−0.46	0	0	−0.3945	−9.2583
3	a	c′	0.00	78.150	2.503	2.437	2.18	0	0	−0.8682	−8.7687
4	a	d′	0.00	77.831	1.615	2.045	1.39	0	0	−0.3061	−8.3843
5	b	a′	8.53	61.470	1.091	0.701	0.98	1	−0.238	−0.3766	−9.8385
6	b	b′	24.45	71.233	0.112	0.379	−0.13	1	−0.238	−0.3698	−9.2712
7	b	c′	3.25	80.158	2.917	2.758	2.50	1	−0.238	−0.8805	−8.7810
8	b	d′	21.15	79.839	2.029	2.367	1.72	1	−0.238	−0.2825	−8.3940
9	c	a′	65.5	96.595	3.474	2.959	3.59	1	−0.278	−0.0551	−8.9809
10	c	b′	57.96	106.36	2.495	2.713	2.48	1	−0.258	0.1849	−8.5192
11	c	c′	66.82	115.28	5.300	4.959	4.89	1	−0.277	−0.7849	−8.8634
12	c	d′	67.28	114.96	4.412	4.683	4.33	1	−0.279	0.0384	−8.8011
13	c	e′	64.65	103.68	2.141	3.077	2.15	1	−0.279	0.0374	−8.9199
Trolox	–	–	38.10	67.793	3.230	3.164	3.19	1	−0.278	−0.0458	−9.0484

[a]Percent inhibition of lipid peroxidation (in vitro).
[b]Total molar refractivity (MR).
[c]Hydrophobicity from Apex–3-D.
[d]Log *P* calculated from CLOGP program.
[e]Log *P* calculated from Molgen program using Crippen's method.

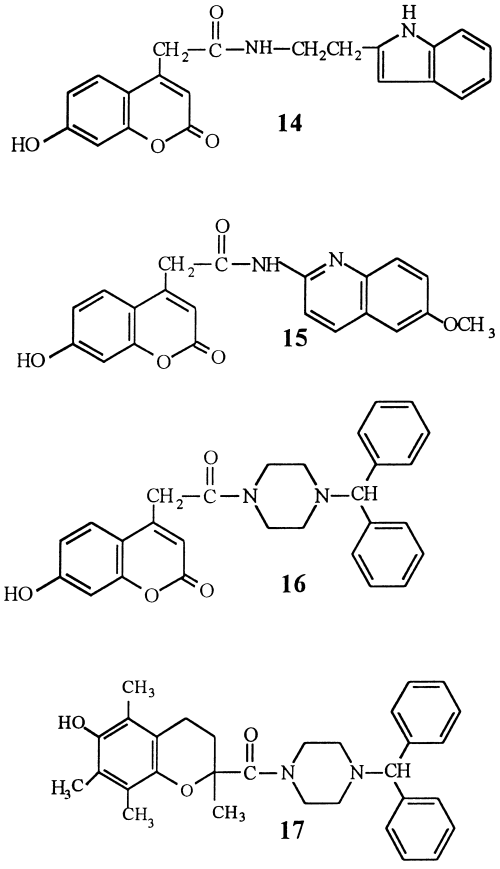

Figure 1. New compounds for testing the derived QSAR models.

similar conditions. ESR-spin trapping of PBN/•OH adducts in the presence of the synthesized chroman and coumarin amides was studied. All compounds suppressed the hydroxyl radical generation resulting in the decrease of signal area of PBN/•OH adduct, suggesting that both chroman and coumarin amides were antiradical.

Biological evaluation

To test the predictive ability of the derived QSAR models, the ability of **14**–**17** to inhibit lipid peroxidation in mouse brain homogenate was determined in vitro using the thiobarbituric acid (TBA) method. The ex vivo lipid peroxidation in the mouse brain after traumatic injury was also measured to investigate the role of antiradicals in cerebroprotection. All of the test compounds showed in vitro inhibitory action against lipid peroxidation. Coumarin amides showed inhibitory activity with IC_{50} of 109–286 μM. Chroman **17** was the most active compound with IC_{50} of 0.17 μM, which was 330 times more potent than trolox, the reference compound. In ex vivo study, the results from injury-head model were in agreement with the results in normal mice. Significant inhibition was not found in coumarin amides even at high dose of 200 mg/kg. On the contrary, the chroman amides showed significant inhibition at a dose of 50–150 mg/kg.

Results and Discussion

Classical QSAR

By stepwise multiple linear regression analysis (MLR), the classical QSAR models were generated with all combinations of property descriptors: log P, MR, E_{LUMO}, E_{HOMO}, OH-indicator and C_{OH} (Table 1). The best models obtained from conventional QSAR study were represented by the following equations.

$$\begin{aligned}\text{Log}(\%\ \text{inhibition}) &= 0.019(\pm0.049)\log P \\ &+ 0.418(\pm0.202)E_{LUMO} - 12.878(\pm0.675)C_{OH} \\ &- 1.815(\pm0.154) \\ &(n = 14,\ r^2 = 0.986,\ S = 0.266,\ F = 233.612, \\ &Q^2 = 0.962,\ S_{PRESS} = 0.369)\end{aligned} \quad (1)$$

$$\begin{aligned}\text{Log}(\%\ \text{inhibition}) &= 0.005(\pm0.003)\text{MR} \\ &+ 0.373(\pm0.179)E_{LUMO} - 12.624(\pm0.558)C_{OH} \\ &- 2.214(\pm0.282) \\ &(n = 14,\ r^2 = 0.989,\ S = 0.202,\ F = 293.065, \\ &Q^2 = 0.974,\ S_{PRESS} = 0.307)\end{aligned} \quad (2)$$

The two models contained three similar independent variables: the electronic descriptors, C_{OH} and E_{LUMO}, and either log P or MR. The most important descriptor was C_{OH} as it was the first selected term. The second descriptor being selected was E_{LUMO} and the third term was log P or MR. The classical QSAR models suggested that the activity (% inhibition of lipid peroxidation) could be improved by increasing the charge of the hydroxyl function in the aromatic ring to a more negative value to increase the reactivity of the functional group (OH) on free radicals; secondly, increasing E_{LUMO} to more than zero; and lastly adding a bulky and/or lipophilic group to enhance the transportation of the drug to the site of action.

Table 2. Melting point and percentage yield of the synthesized compounds

Compound	Formula	Recrystn solvent	Mp[a] (°C)	Yield (%)	Analyses[b]
14	$C_{21}H_{18}N_2O_4$	Ethanol:water	136–138	20.48	C, H, N
15	$C_{21}H_{16}N_2O_5{\cdot}1/2H_2O$	Ethanol:water	235–237	12.67	C, H, N
16	$C_{28}H_{26}N_2O_4$	Ethanol:water	250–251	29.31	C, H, N
17	$C_{31}H_{36}N_2O_3{\cdot}1/2H_2O$	Ethanol:water	184–185	32.30	C, H, N

[a]No attempts were made to optimize yield.
[b]Analyses for C, H, N were within ± 0.4% of the theoretical value required.

When QSAR of the subset of chroman amides **9**–**13** was determined, the best equation was

$$\begin{aligned}\text{Log}(\%\ \text{inhibition}) &= 0.007(\pm 0.000)\log P \\ &+ 0.022(\pm 0.001)E_{\text{HOMO}} - 2.779(\pm 0.015)C_{\text{OH}} \\ &- 1.213(\pm 0.003) \\ &(n = 5, r^2 = 1.000, S = 9.44 \times 10^{-5}, F = 103560.591, \\ &Q^2 = 0.963, S_{\text{PRESS}} = 0.1800)\end{aligned} \quad (3)$$

The electronic C_{OH} was firstly selected, followed by log P and E_{HOMO}, respectively. It was the same as eqs (1) and (2) that the electronic descriptor, C_{OH}, was the most important for the molecular design of radical scavenger. For other electronic descriptors, electron donating ability of the molecule (E_{HOMO}) was one of the significant factors in eq (3) instead of E_{LUMO} in eqs (1) and (2). These revealed that the radical scavenging ability was attributed to the capacity of the molecule to donate electron as well as to accept the electron.

3-D–QSAR pharmacophore generation

In the 3-D–QSAR study using Apex–3-D program, the first step was to minimize 14 structures by the conjugated method followed by importing the minimized energy structures. The program automatically created numbers of biophore models (pharmacophores) from hydrophobic, steric and electronic parameters. Besides global properties, descriptors representing the properties of secondary sites were added to the biophore model to improve the statistics. The single conformer of minimized structure was used in derivation of 3-D–QSAR model in the beginning, but the statistical values of the obtained models were not satisfactory. Therefore, single conformer with minimized energy of each compound was replaced by multiple conformers. The minimized structures were rotated around every important single bond to generate the conformers. A large number of conformers from each compound was clustered into groups of main conformation for conformer selection. Five to 15 conformers representing the different types of conformers were chosen by clustering procedure, the Apex–3-D model 1, one of the two best models obtained from a data set of 13 compounds, and trolox was deduced from the original data set as the outliner. The equation of Apex–3-D model 1 is as follows.

$$\begin{aligned}&\%\ \text{Inhibition} = 4.748(\pm 1.59)\text{CLOGP} - 27.621(\pm 4.30) \\ &\text{hydrophobicity site 2} - \\ &12.847(\pm 1.25)\text{refractivity sites 3} \\ &+ 2.399(\pm 0.91)\text{refractivity site 4} + 46.493(\pm 4.41) \\ &(n = 13, \text{RMSE} = 4.94, \text{RMSP} = 6.82, Q^2 = 0.94, \\ &r^2 = 0.98)\end{aligned} \quad (4)$$

The statistics in expression of analysis in Apex–3-D model were root mean square error (RMSE) and predictive root mean square error (RMSP) and correlation coefficient of standard regression (r^2) and Q^2. The Apex–3-D biophore model 1 was composed of three biophores (Fig. 2): (i) pyran in the chroman nucleus or the pyridine ring of nicotinic nucleus, (ii) O atom of amide function and (iii) N atom of amide function. The attributed properties were the same lipophilic and steric descriptors as in the classical QSAR model. However, the hydrophobicity and steric properties at secondary sites 2 and 3 of Apex–3-D model 1 (Fig. 3) were not favored due to the negative values of their coefficients. The disfavored effects from sites 2 and 3 contributed to the low activity as shown in compounds **6** and **10** that contained propylmorpholine, and compound **11** that contained a quinoline side-chain. Disfavorable secondary site 2 was located at the propylene aliphatic between the amide and the morpholine side-chain, including position C10 of the quinoline ring. Disfavorable site 2 was not found in amide containing ethylindole and ethylpiperazine side-chains, which had good activity. These suggested that the distance between the ring system of side-chain and the amide function was critical. The most appropriate distance should be approximately 1–2 carbons of aliphatic chain. The disfavorable secondary site 3 of Apex–3-D model 1, which was the steric refractivity, was located at position C2 of the chroman

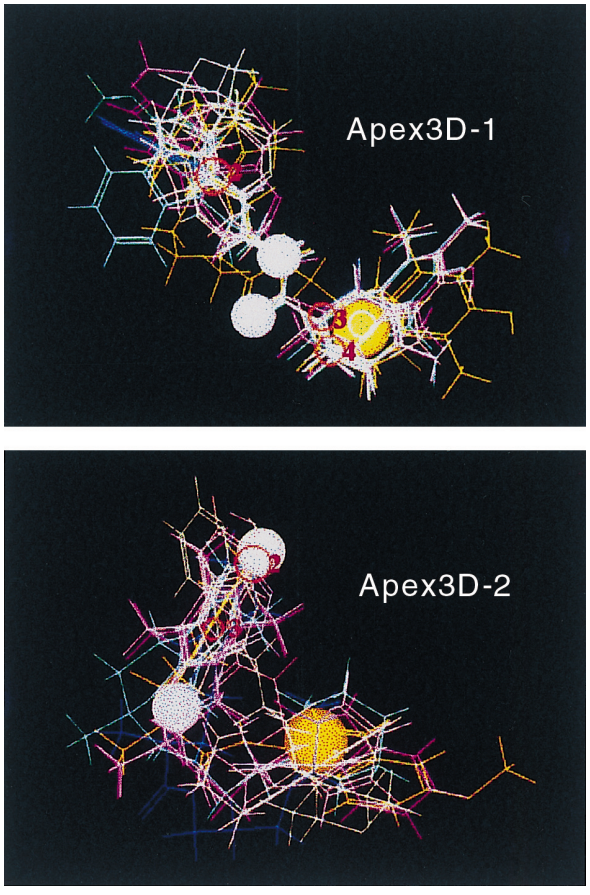

Figure 2. Superimposition and 3-D biophore models of Apex–3-D.

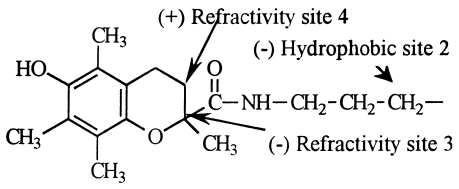

Figure 3. Diagrammatic representation of the secondary sites of Apex–3-D model 1.

portion. Too much refractivity or bulk at this site would cause the conformation of chroman to deviate from planarity. However, a positive coefficient of secondary site 4 suggested that great refractivity or a large substituent at this site would increase the activity. It seems that the sizes of substituents at sites 3 and 4 have to compromise in order to obtain planarity of the fused ring for accommodation of electron transfer and delocalization.

The attempts had been made to optimize the statistical values by eliminating the outliers **3**, **4**, **6** and **7** and the improved Apex–3-D2 equation was obtained. The equation of Apex–3-D2 is as follows.

$$\begin{aligned}&\%\ \text{Inhibition} = 4.461(\pm 1.13)\text{CLOGP} + 9.923(\pm 0.93)\\ &\text{refractivity site } 2 + 45.017(\pm 3.81)\text{ring PRESENCE}\\ &\text{site } 3 - 1.161(\pm 0.13)\\ &(n = 9,\ \text{RMSE} = 3.02,\ \text{RMSP} = 4.07,\ Q^2 = 0.97,\\ &r^2 = 0.99)\end{aligned} \tag{5}$$

There were three biophores in Apex–3-D model 2 (Fig. 2) which was composed of: (i) hydroxyl group of aromatic ring or nitrogen of pyridine ring without OH function, (ii) O atom in pyran ring of chroman amides or O atom of amide bearing nicotinic nucleus and (iii) ring system of side chain. It was the same as model 1 that the lipophilicity was the significant effect on the activity. Because of the positive coefficient indicator variable (ring presence site 3 of Apex–3-D2 model), the aromatic ring containing OH was essential for the inhibitory effect.

3-D–QSAR CoMFA

CoMFA, one of the most powerful tools for QSAR and drug design, was employed in this study. In alignment procedure, the superimposition was used to align the molecules to the template molecule, compound **12**. The chosen atoms for superimposition alignment were hydroxyl group and aromatic ring of nucleus, nitrogen and oxygen atom of amide function and heteroatom on ring system of side chain. The CoMFA standard probe, a hybridized carbon atom with a +1 charge, sp^3 *C* (+1) (CH_3 for steric and a positive charge for electrostatic), was used in parallel with other probes such as *H* (+1), sp^3 O (−1) and sp^3 O (−2). The sp^3 C (+1) probe yielded the higher cross-validated r^2 (Table 3). The contributions from steric and electrostatic fields were 42.3% and 57.7%, respectively.

The CoMFA steric and electrostatic fields were displayed as a contour map (Fig. 4). The green contour regions were favorable and the yellow regions were disfavorable steric space. The located green contours suggested a preference for a CH_3 substituent at the C5 position, in addition to bulky atoms at C2 and C4. There was also favorable steric region corresponding to the location near position O1 and extending to the C3 and C4 positions of the pyran ring. Besides the favorable green region, a small disfavored yellow contour was found near C3 and C4. These results may indicate that increased activity requires the optimum steric properties around the pyran and amide functions to complement the planarity of the pyran or cyclic nucleus in relation to the aromatic hydroxy and carbonyl amide functions. The planarity will increase the electron transfer capacity and delocalization, leading to improved radical scavenging ability. A few large yellow contour regions near the amide function and ethylene group between the chroman and indole rings indicated that substitution on the chain between the nucleus ring and the side chain ring would decrease the activity.

Table 3. Statistical parameters of CoMFAs from different probe atoms

Probe atoms	Cross-validation			QSAR regression			Contribution (%)	
	Q^2	S_{PRESS}	noc[a]	r^2	*S*	*F*	Steric	Electronic
Sp^3 C (+1)	0.794	16.189	5	0.998	1.474	1006.865	42.3	57.7
Sp^3 H (+1)	0.659	19.970	4	0.994	2.792	348.944	47.8	52.2
Sp^3 O (−1)	0.711	18.703	4	0.994	2.629	393.771	48.6	51.4
Sp^3 O (−2)	0.719	18.281	4	0.994	2.691	375.709	52.0	48.0

[a]Number of component.

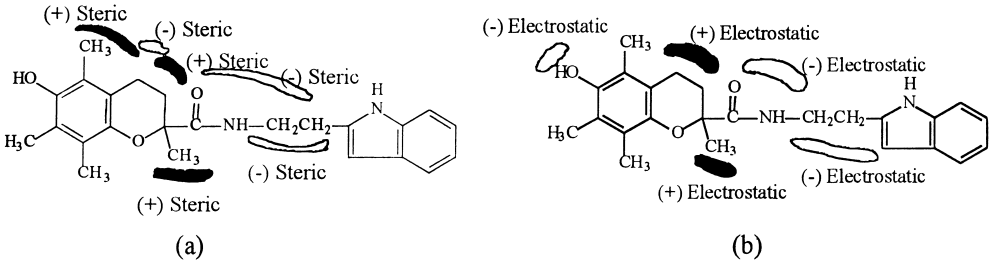

Figure 4. Diagrammatic representation of CoMFA contour maps: (a) steric and (b) electrostatic fields.

The electrostatic contribution contour map showed a small red area at the hydroxyl group substituted on C6 of the chroman portion, which suggested that the presence of an electron-donating group or high electron density on this site increased the activity. This was in agreement with the classical QSAR studies, which showed that the active compound required the high negative charge of an oxygen atom at the hydroxyl function. Two small red regions, under the O and N atoms of the amide function, and one large red area close to the aliphatic chain between the amide function and indole ring in the electrostatic contour map, revealed that high electron densities were preferred for these sites. A large blue region in the electrostatic contour map corresponding to the C3 and C4 positions of the chroman portion probably indicated that an electron-withdrawing substituent or positive charge was preferred on these positions. There was an electron-withdrawing region corresponding to the location near the methyl substituted on C2 position of pyran and extending to the carbonyl group of the amide function.

Comparison of QSAR equations

The models were validated using statistical approaches together with real prediction. The statistical approaches were the correlation coefficient (r^2) characterizing the overall fit, and the predictive power of the model, cross-validated correlation coefficient or Q^2 (Table 4). The five models derived from classical QSAR and 3-D–QSAR procedures yielded significant predictive cross-validated r^2 higher than the accepted value (0.3). The scatter plots of experimental percent inhibition of lipid peroxidation in vitro against predicted values of 3-D–QSAR models and CoMFA model are shown in Fig. 5.

Predictive ability

In addition to the lateral validation of QSAR, the derived models were tested by being used to predict the activity of new compounds **14**–**17** (not including in the training set) and **12**. New **14**–**16** contained coumarin group which was not in the training set, while the new **17** and the former **12** contained chroman which was the functional group in the training set. The predicted activity was the percent inhibition of lipid peroxidation at 50 μM; the experimental values were in vitro IC_{50} as the inhibitory action of **12** and **17** were greater than 100% at 50 μM. The protocol to evaluate antilipid peroxidation was slightly modified. Pig brain in the previous study was replaced by mouse brain and the detection method was spectrofluorometry instead of spectrophotometry. The modification was made to reduce the sample size and to increase the sensitivity in order to suit the ex vivo test. Regardless of these differences, the predicted values were found to be in agreement with the experimental values (Table 5). Compound **17** was predicted to be the most active compound, as was found experimentally. The linear correlations between the predicted activity (percent inhibition) and the experimental IC_{50} were determined to support the predictive ability of the derived models. The correlation coefficients were high in all models but the relationship was significant only in classical and Apex–3-D 2 models (Table 6).

Classical 2 and Apex–3-D 2 models yielded good prediction, potent activity for **17** and low to medium activities for **14**–**16**. The classical QSAR models made good physicochemical sense that antilipid peroxidation by scavenging radicals was attributed to the electronic C_{OH} and E_{LUMO}, steric MR and hydrophobic log P. The activity of compound **17** predicted by the CoMFA model was only 44%, whereas experimentally it was potent (>100%). This deviation is possibly due to the missing hydrophobic field. The fields produced by the standard CoMFA probe are only electronic (coulombic) and steric (van der Waals), while steric, electronic and hydrophobic effects are considered to be important for biological activity. Numerous techniques were therefore established in order to include the hydrophobic effect, such as the hydrophobic interaction technique (HINT), grid field and addition of H_2O probe to represent H-bonding field. The activity in this study was measured in brain lipids, where the hydrophobic property is significant for accessibility. The discrepancy of the CoMFA prediction from the experimental values, especially for compound **17**, was therefore due to the missing hydrophobic field in the standard CoMFA study.

Table 4. Comparison of QSAR statistical results

Models	QSAR regression		Cross-validation		noc[a]	Components
	r^2	S (RMSE)	Q^2	S_{PRESS} (RMSP)		
QSAR ($n=14$)						
classical-1	0.986	0.226	0.962	0.369	3	E_{LUMO}, C_{OH}, log P
classical-2	0.989	0.202	0.974	0.307	3	E_{LUMO}, C_{OH}, MR
3-D–QSAR						
Apex–3-D 1 ($n=13$)	0.982	4.942	0.944	6.818	4	Global CLOGP hydrophobic site 2 steric refractivity sites 3, 4
Apex–3-D 2 ($n=9$)	0.994	3.017	0.978	4.074	3	Global CLOGP steric refractivity site 2 ring presence indicator
CoMFA ($n=14$)	0.998	1.474	0.794	16.189	5	Steric, electrostatic effects

[a]Number of component.

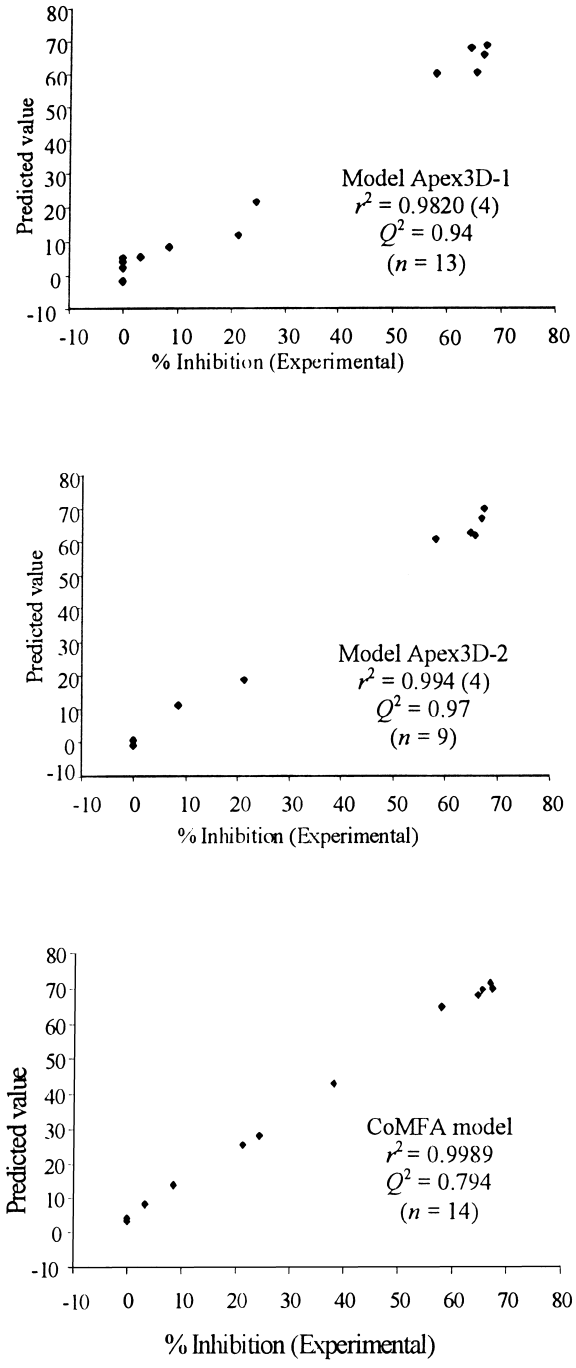

Figure 5. Plots of experimental versus predicted percent inhibition of lipid peroxidation. Predicted values were calculated from Apex–3-D 1 and Apex–3-D 2 and CoMFA models, leave-one-out cross-validated r^2 (Q^2) given along with number of components in parentheses.

In conclusion, the major structural properties contributing to the activity in 3-D–QSAR models derived from Apex–3-D program were lipophilicity, the optimum steric property and the geometry of the side chain. It appeared that the distance between the ring system in the amine portion and the nucleus ring of the acid part should be optimized. The aromatic ring of the nucleus portion containing an hydroxy group should be substituted to provide the inhibitory effect. Furthermore, steric and/or bulky properties of atoms and substituents in the pyran ring to accommodate the planarity were important for electron transfer resulting in the inhibition of lipid peroxidation activity.

Ex vivo antilipid peroxidation

Test compounds were further evaluated for ex vivo antilipid peroxidation in mice at a dose range from 50 to 200 mg/kg subcutaneously administered. One hour after injection, the mice were killed and the brain was excised for the evaluation by using thiobarbituric acid method. The results showed that only chroman amide **17** significantly inhibited lipid peroxidation at the doses of 100 and 150 mg/kg. It was contrary to coumarin amides **14**–**16** for which significant inhibition was not found even at higher dose of 200 mg/kg.

Investigation of the activity under the condition that led to overproduction of radicals was also carried out. Compounds **14** and **17** were selected for the ex vivo studies by using the injury-head model. In this model, unanesthetized male mice were subjected to concussive head injury (approximate force of 1500 g-cm) that was produced by a 100 g weight dropped from a height of 15 cm. The test compounds were administered subcutaneously at 5 min after injury. At 1 h after injection, the mice were killed and the brains were excised quickly to evaluate antilipid peroxidation activity. The thiobarbituric acid reactive species in traumatic brain after head injury was higher than control; percent increase was 11.44% ($P < 0.01$). This indicated that traumatic injury increased radical generation, and lipid peroxidation went up when head injury occurred. The results from ex vivo study in injury-head model were in agreement with the ex vivo results in normal mice (Table 7). Chroman amide **17** gave percent inhibition of 23.80% at the dose of 100 mg/kg while coumarin amide **14** was still inactive. The test compounds appeared to be more efficient when radicals were in excess.

ESR studies

As $^{\bullet}$OH radical is the predominant radical contributing to cellular damage in biological systems, the ability of chroman and coumarin amides to trap $^{\bullet}$OH was evaluated. Reaction of **14**–**17** and $^{\bullet}$OH was investigated by the ESR spin trapping method. The result showed that chroman **17** reacted with $^{\bullet}$OH yielding chromanoxyl radicals, as observed in Figure 6. Chromanoxyl radicals of **17** was found to decay over time, the area of its signal decreased by 21% after standing for 20 min (signal areas at 5 and 25 min were 343 and 271 Ms, respectively). On the contrary, there was no ESR signal from all coumarin amides under similar experimental conditions. This suggested the possibility that coumanoxyl radical was not stable to be detected directly or the non-hindered hydroxyl radical of coumarin amide easily reacts with other species.

ESR spin trapping studies of PBN/$^{\bullet}$OH adduct in the presence of synthesized compounds were further conducted to support the scavenging ability of **14**–**17** against radicals. It appeared that all compounds suppressed the $^{\bullet}$OH generation resulting in the decrease of signal area of PBN/$^{\bullet}$OH, as presented in Figure 7. Formation of

Table 5. The predicted activity from QSAR models and the experimental activity

Compounds	Predicted values[a]					Experimental[b]	
	Classical QSAR		3-D QSAR			Inhibition %	IC_{50}
	1	2	Apex–3-D 1	Apex–3-D 2	CoMFA	(50 μM)	(μM)
12	75.67	92.29	68.73	69.77	70.03	> 100	0.31
14	16.03	20.61	23.22	19.08	21.57	12.09	109.52
15	4.82	6.56	23.53	11.97	11.07	35.14	286.14
16	19.36	33.03	52.14	22.54	14.39	38.86	156.27
17	59.22	99.17	82.90	85.30	44.18	> 100	0.17

[a]Percent inhibition against lipid peroxidation.
[b]Mouse brain was used as lipid source in the present experimental test whereas pig brain was used in the previous study.

Table 6. Statistical parameters of QSAR models and the correlation of predicted activity versus the experimental activity

	Classical 1	Classical 2	Apex–3-D 1	Apex–3-D 2	CoMFA
QSAR regression r^2	0.986	0.989	0.982	0.994	0.998
Validation Q^2	0.962	0.974	0.944	0.978	0.794
Correlation r^2 (P-value)					
predicted versus IC_{50}	0.804	0.822	0.639	0.767	0.713
	(0.03)	(0.03)	(0.10)	(0.05)	(0.07)
predicted versus inhibition	0.858	0.897	0.843	0.895	0.861
	(0.02)	(0.01)	(0.02)	(0.01)	(0.13)

Table 7. Antilipid peroxidation activity and scavenging ability against •OH

Compounds	Lipid peroxidation (TBA method)			Percent reduction of PBN/•OH (5 mM)	Log P
		Ex vivo, percent inhibition[a] (100 mg/kg)			
	In vitro IC_{50} (μM)	Brain assay ($n = 6$)	Injured brain assay[b] ($n = 5$)		
14	109.52	NA	NA	47.37	1.76
15	286.14	NA	—	38.87	2.55
16	156.27	NA	—	61.13	3.65
17	0.17	13.01*	23.80*	48.92	6.21

[a]The inhibition of ex vivo lipid peroxidation was measured in brain homogenates 1 h post administration.
[b]Test compound or vehicle was administered subcutaneously after a concussive head injury (force of 1500 g-cm). *$P < 0.01$ versus vehicle treated controls; NA, no activity.

spin adduct of PBN/•OH was evidenced by the appearance of the characteristic 2:2:2 ESR hyperfine splitting pattern (g-value = 2.0056, a_N = 14.3 G, a_H = 2.7 G). Among the coumarin amides, **16** is the most effective that showed percent reduction of signal area of PBN/•OH of 61.13 at 5 mM concentration, while **14** and **15** gave percent reductions of 47.37 and 38.87, respectively (Table 8). Since ESR signals of chromanoxyl radical of **17** partly overlapped signals of PBN/•OH adduct, the area measurements were made only in the region of the unoverlapped signal. Chroman and coumarin amides were found to inhibit the PBN/•OH adduct signal area in a concentration dependent manner. The effectiveness in the suppression of •OH radical leading to decrease in PBN/•OH signal strongly suggested that chroman and coumarin amides were antiradicals. Coumarin amides possessed the •OH trapping ability as well as chroman amides regardless of no coumanoxyl ESR

Table 8. Effect of test compounds on the ESR signal areas of PBN/•OH adduct[a]

Compounds	Test compounds (mM)	Peak area of PBN/ •OH adduct (Ms)	Percent reduction of PBN/ •OH adduct
14	5	50.1	47.37
	10	44.0	53.73
15	5	58.2	38.87
	10	42.1	55.78
16	5	37.0	61.13
	10	33.5	64.81
17[b]	5	27.80[b]	48.92
	25	13.20[b]	72.89

[a]The ESR spectra were recorded at 5 min after adding a mixture of PBN (25 mM) and different concentrations of test compounds to $H_2O_2/CuSO_4$ system.
[b]Partial peak areas of PBN/•OH adduct that were not overlapped with the •OH adduct of the test compounds.
The assays were run in duplicate and the difference was less than 10%.

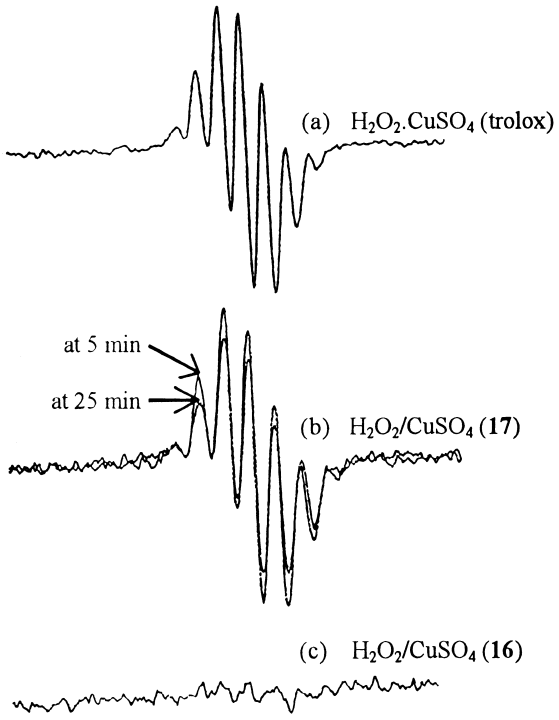

Figure 6. The ESR spectra after adding test compounds (5 mM) to •OH generated from $H_2O_2/CuSO_4$ system: (a) trolox, (b) chroman amide **17** and (c) coumarin amide **16**.

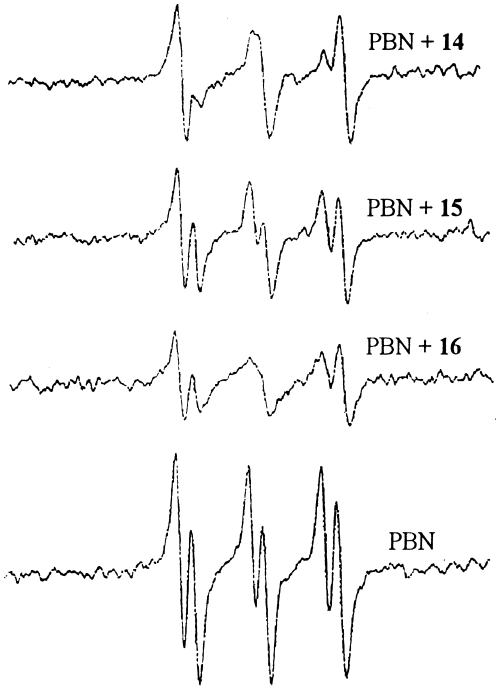

Figure 7. Effect of coumarin amides **14**–**16** on the formation of PBN/•OH adducts. ESR spectra were obtained 5 min after addition of PBN (25 mM) or mixture of PBN (25 mM) and coumarin amides (5 mM) to the system.

signals. It is likely that coumarin amides cannot function as prooxidant since their radicals (coumanoxyl radicals) are either weak or not stable to be detected by ESR.

The results of antilipid peroxidation activity both in ex vivo and in vitro and ESR studies are summarized in Table 7. It was found that coumarin amide series (**14**–**16**) were not effective ex vivo whereas the in vitro and ESR results indicated the antilipid peroxidation activity and radical-scavenging ability. The discrepancies between the in vitro and ex vivo results might be because of the poor access to the brain. The non-hindered hydroxyl group in coumarin nucleus was not only metabolically unstable but also prone to react with various species in the biological system. Moreover, coumarin amides also had low log *P* that affected their ability to cross the blood–brain barrier.

Conclusions

The relationships between structure/physicochemical property and in vitro lipid peroxidation inhibitory activity of 13 previous compounds were studied by both classical QSAR and 3-D–QSAR techniques.

From classical QSAR, two best models with Q^2 of 0.96 and 0.97 were obtained; the two models contained three similar independent variables. The two variables were the same electrostatic descriptors, charge of hydroxyl group on aromatic ring (C_{OH}) and E_{LUMO}. The third variable was either lipophilic log *P* or steric MR as the high lipophilic log *P* and steric MR appeared to be highly intercorrelated.

Three 3-D–QSAR models of high Q^2 (0.94, 0.97 and 0.79) were obtained using 3-D pharmacophore generation (Apex–3-D program) and comparative field analysis (CoMFA) techniques. For Apex–3-D studies, structure properties contributing to the activity were not only lipophilic but also the optimum steric and geometry of both nucleus and side chain's composition to accommodate the planarity for electron transfer. For CoMFA studies, the hybridized carbon with a +1 charge probe, sp^3 *C* (+1), yielded the best Q^2 of 0.794 with steric and electrostatic contributions of 42.3 and 57.7%, respectively. The increased activity required the optimum steric properties around the pyran to complement the planarity of pyran or cyclic nucleus. In addition, the presence of electron donating or high electron density at hydroxyl group on aromatic ring of chroman portion accounted for the activity. Hydrophobic and steric properties are the important factors in Apex–3-D models while electronic effect and steric effect gave almost equal contributions to the activity in the CoMFA model.

It was apparent from all models that the descriptors that affected the electronic property of the molecule are most important for the design of radical scavengers. These descriptors are electronic descriptors (C_{OH}, E_{LUMO} and E_{HOMO}) and steric descriptors that affected the electrostatic property or electron transfer of the molecule. However, lipophilicity is also a significant factor and should be included in the molecular design to assure the availability of the drug at the target site.

The predictive power of the models derived from QSAR studies was tested by the four new compounds **14**–**17** and one compound in the training set. Compounds

14–16 contained coumarin, the new functional group. The most potent compound in the training set, chroman **12**, was included in this testing as there was discrepancy in the protocol of biological evaluation. The predicted activity in terms of percent inhibition was in fair agreement among the derived models. The linear correlations between the predicted percent inhibition and the experimental IC_{50} or percent inhibition were high; only the classical and Apex–3-D models gave significant correlation. Regardless of the limited data, the derived relationships were indicative of trend no matter whether percent inhibition was used to derive the relationship instead of the customary IC_{50} or the protocol of biological testing was slightly modified. The predicted activity in terms of percent inhibition which was a biological end point of a single dose was found to correlate or could extrapolate to IC_{50}, the end point that reflected a response at several doses. These indicated that the statistical relationship was predictive.

The conventional QSAR models and 3-D–QSAR models from Apex–3-D program had better predictive power than models derived from CoMFA. This can be explained since all important properties (steric, electrostatic and hydrophobic properties) contributing to the biological activity were included in the generation of 3-D–pharmacophore and QSAR models by Apex–3-D program whereas hydrophobic effect was not included in the standard CoMFA.

In in vitro lipid peroxidation assay, all test compounds showed inhibitory action against lipid peroxidation. The IC_{50}s of coumarin amides **14–16** were 109–286 μM. Chroman **17** was the most active compound with IC_{50} of 0.17 μM, which was 330 times more potent than trolox. In ex vivo assay, the result from the injury-head model was in agreement with the result in normal mice. Significant inhibition was not found in coumarin amides even at high dose of 200 mg/kg. It was contrary to chroman amides **17** which showed significant inhibition.

ESR-spin trapping study was performed to investigate the scavenging ability of test compounds against hydroxy radical. Chroman derivatives reacted with hydroxyl radical yielding ESR signals of chromanoxyl radicals, whereas ESR signal was not found from all coumarin amides under similar conditions.

ESR-spin trapping of PBN/$^{\bullet}$OH adducts in the presence of the synthesized chroman and coumarin amides was investigated. All compounds suppressed the hydroxyl radical generation resulting in the decrease of signal area of PBN/$^{\bullet}$OH adduct, suggesting that both chroman and coumarin amides were radical scavengers.

From lipid peroxidation assay and ESR-spin trapping studies, it appeared that compounds in coumarin series were not effective ex vivo despite their good inhibitory action in vitro against lipid peroxidation and ESR radical scavenging ability. The difference between in vitro and ex vivo results was possibly arisen from the poor access of coumarin amides in the target organ, brain, due to low log *P*. The non-hindered hydroxyl group in coumarin nucleus was not only metabolically unstable but also prone to react with various species in the biological system. Thus, the structure/physicochemical properties for good bioavailability should also be taken into consideration in drug design.

Experimental

Biological data for QSAR study

The in vitro percent inhibition of lipid peroxidation by the 13 previously synthesized compounds and trolox was used as the dependent variable.

Classical QSAR study

The selected structure and physicochemical properties used were molecular orbital energy (E_{LUMO} and E_{HOMO}), charge, lipophilicity (log *P*, total hydrophobicity) and total refractivity (MR). The structures were minimized using the conjugation method and then subjected to full energy optimization using semi-empirical AM1 Hamiltonian in MOPAC program (Interface/MOPAC option of Sybyl 6.3).[23] The electronic descriptors were molecular orbital energy (E_{LUMO} and E_{HOMO}) and charge of hydroxyl group (C_{OH}). The hydrophobic or lipophilic descriptors were the log *P* calculated from CLOGP program in the previous study or log *P* determined from program Molgen 4.0. MR was obtained from Apex–3-D program (Insight II release 95.0).[22] The intercorrelations between these independent descriptors were determined to avoid colinearity. Regression analysis was performed on a Pentium-133 Mz PC using multiple linear regression (MLR) in SPSS for Windows Release 7.[24]

3-D–QSAR pharmacophore generation

3-D models of chemical structures were built by molecular modeling program Insight II release 95.0 (Apex–3-D module) on Silicon Graphics Indy workstation. Structures of all compounds were minimized using conjugation method, then the charge potential was fixed. The conformations of lowest energy were then generated. Multiple conformations were generated by performing a systemic search of all rotable bonds. The number of conformations was reduced to the required number using a conformation clustering option. A set of molecules was entered into the task's database in the Apex–3-D module. Compounds were classified into three levels of activity for entry in the Molecular Definition Table: good activity for compounds showing percent inhibition $>50\%$, intermediate activity for compounds showing percent inhibition of 30–50% and low activity for compounds showing percent inhibition $<30\%$. In addition to global structure properties for QSAR analysis, the extra property data (such as CLOGP) and indicator variables (OH-indicator) were added to the task's database. The default set was chosen for the descriptor centers and the distance criterion for identifying biophores (pharmacophores). The biophore model was identified with the resulting biophoric superimposition. QSAR models were initially built based on biophore sites and

global properties, then refined using properties of secondary sites, such as atomic partial charge (heteroatom), hydrophobic sites, steric sites and ring presence.

3-D–QSAR CoMFA

The 3-D structures of compounds were constructed using Sybyl version 6.3[23] on SGI Power Challenge XL. Conjugation method was used to minimize structures as the starting point; the geometry was optimized by semi-empirical AM1 calculation. The superimposition option was used to align the molecules to the template molecule. Compound **12**, which had the highest activity, was used as the template. The chosen atoms for superimposition alignment were the hydroxyl and aromatic ring of the nucleus, the oxygen and nitrogen of the amide function, and the heteroatom on the ring of the side chain. The CoMFA fields, both steric and electrostatic, were created using Tripos Standard CoMFA Field Class. The probe atom was placed at each lattice point and the interactions of the steric and electrostatic fields for each atom in molecule were all calculated with CoMFA standard scaling and then compiled in a CoMFA QSAR. A statistical analysis of the resulting set of grid point interaction energies by the partial least squares (PLS) method was performed. A cross-validated analysis was employed both to determine and optimize the cross-validated r^2 (Q^2) and the optimum number of components for the model. The analysis was rerun without cross-validation using the optimum number of components to determine the standard regression statistics.

Statistical method

Stepwise MLR was used to develop the classical QSAR model. The reliability and predictive ability of the model were considered by multiple correlation coefficients (r^2), standard deviation (S), F-test values and predictive r^2 or cross-validated r^2 or Q^2. The statistics in expression of analysis in Apex–3-D model were root mean square error (RMSA) and predictive root mean square error (RMSP) and correlation coefficient of standard regression (r^2) and Q^2. PLS methodology implemented in Sybyl was used to perform the correlation between the steric and electrostatic properties (independent variable) and inhibitory activity. Cross-validation (leave-one-out method) and a non cross-validated analysis were used to analyze the CoMFA models. The overall predictive ability of the analyses was expressed in terms of the predictive r^2 or Q^2. The uncertainty of the prediction was expressed in terms of S_{PRESS}.

Synthesis

Melting points of the compounds were determined on a Buchi capillary mp apparatus and uncorrected. IR spectra were run on an FTIR Nicolet 500 as a potassium bromide pellet. ^{1}H NMR spectra were obtained with a Jeol JNM-A-500 (500 MHz). Chemical shifts were reported in ppm relative to the internal standard, tetramethylsilane. MS was done using a Jeol FX 900 (90 MHz). Thin layer chromatography (TLC) was carried out on Merck Kieselgel 60 F_{254} plates and the purified compounds each showed a single spot. Chromatographic purification was performed on silica gel columns; the silica gel used for column chromatography was Merck Kieselgel 60 of 0.063–0.200 mm. Analytical results obtained from an elemental analyzer (Perkin–Elmer PE 400) were within ±0.4% of the theoretical value for all compounds. Spectral (IR, MS, NMR) data were compatible with the assigned structures in all cases.

The general procedures for the synthesis of the amides involved the reaction of selected carboxylic acids with the amino compounds by coupling with *N,N′*-carbonyldiimidazole (CDI). All starting materials were commercially available except 2-amino-6-methoxyquinoline which was prepared by the reported method.[25] Representative method used to prepare the target amides is described in the following example.

Synthesis of 17. Carbonyldiimidazole (0.162 g, 1 mmol) was added in small portion to a solution of trolox (0.250 g, 1 mmol) in THF (6 mL) and the mixture was stirred for 2 h at room temperature. Then, diphenylmethylpiperazine (0.252 g, 1 mmol) in THF (4 mL) was added dropwise to the stirring mixture. The reaction mixture was stirred at room temperature for 24 h and then evaporated to dryness under reduced pressure. The resulting residue was purified by passage through a silica gel column (chloroform:methanol, 7:1). Recrystallization from ether gave compound **17**, 0.313 g (32.30% yield), mp 184–185 °C. IR (KBr) (cm^{-1}): 3460 (OH), 3080–2973 (aromatic CH), 2920–2854 (aliphatic CH), 1624 (C=O), 1499–1433 (PhC=C), 1453 (N-CO), 1242 (C-N), 1216–1104 (C-O), 755, 709. ^{1}H NMR ($CDCl_3$): δ 1.53 (s, 3H, 2-CH_3), 1.70 (m, 1H, H3$_a$), 2.03 (s, 3H, 5-CH_3), 2.05 (s, 3H, 7-CH_3), 2.15 (s, 3H, 8-CH_3), 2.27 (m, 4H, piperazine-2′ and 6′), 2.54 (m, 2H, H4), 2.73 (m, 1H, H3$_b$), 3.41, 3.62, 3.92 and 4.02 (m, 4H, piperazine-H3′ and 5′), 4.12 (s, 1H, N-CH-Ar$_2$), 4.23 (s, exchangeable with D_2O, OH), 7.15 (m, 2H, ArH), 4.24 (m, 4H, ArH), 7.35 (m, 4H, ArH). Anal. ($C_{31}H_{36}N_2O_3 \cdot 1/2H_2O$) C, H, N.

In vitro lipid peroxidation assay

The supernatant fraction of pig brain homogenate was prepared according to the method of Stock et al.[26] The diluted homogenate was stored at −80 °C for up to 8 weeks. Lipid peroxidation was assessed by the formation of thiobarbituric acid (TBA)-reactive species (e.g. malondialdehyde) as described previously.[27] Most compounds were prepared in water or water:ethanol and were diluted serially. The percent inhibitions were determined at six concentrations in triplicate. IC_{50} values were obtained from the linear regression plots between the percent inhibition versus concentrations.

Ex vivo lipid peroxidation assay in normal and head-injury model

Groups of 5 male Swiss albino mice (27–33 g) were subjected to a concussive head injury (force of 1500 g-cm). Test compounds (50 mg/kg and 200 mg/kg) or vehicle

were administered subcutaneously after the injury. The brain was excised 1 h post administration of test compound or vehicle and homogenized in ice-cold potassium phosphate buffer (1:19 w/v). The mixture was centrifuged after addition of perchloric acid (35% v/v). Thiobarbituric acid (1% v/v in 50% glacial acetic acid) was added to the supernatant and the mixture was heated to 100 °C for 15 min. The fluorescence of TBA-reactive substances was measured at 515 nm (excitation wavelength) and 553 nm (emission wavelength).

Electron spin resonance study

For evaluation of •OH trapping ability, compounds **14**–**17** were examined as spin traps using ESR spectroscopy and compared to α-pheny-*tert*-butylnitrone (PBN). $CuSO_4/H_2O_2$ reaction was used to generate •OH. Test compound or the mixture of test compound (final concentration, 5–75 mM) and PBN (final concentration, 25 mM) was added to a test tube containing the freshly prepared solution mixture between $CuSO_4$ (final concentration, 0.1 mM) and H_2O_2 (final concentration, 10 mM), and phosphate buffer pH 7.4 was added to a final volume of 1.0 mL. As test compound was dissolved in ethanol and ethanol itself is a •OH trap, thus, controls containing an equal volume of ethanol was used. The spectra were recorded at 5 min after mixing the solution on a Jeol (JES-RE2X) ESR spectrometer with the following parameters: magnetic field strength 335.10 mT, microwave power 20 mW, modulation amplitude 1×1000 mT, time constant 0.1, sweep width 5.0×1 mT, and modulation width 0.5×0.1 mT.

Acknowledgements

The authors thank the Faculty of Pharmacy, Chulalongkorn University for computer facilities (Insight II) and High Performance Computing Center, National Electronics and Computer Technology Center, Bangkok, Thailand for computer facilities (Sybyl 6.3).

References and Notes

1. Halliwell, B.; Gutteridge, J. M. C. In *Free Radicals in Biology and Medicine*; Halliwell, B.; Gutteridge, J. M. C., Eds.; Clarendon Press: Oxford, 1989; 2nd ed., pp 1–20.
2. Roberfroid, M.; Colderon, P. B. In *Free Radicals and Oxidation Phenomena in Biological Systems*; Roberfroid, M., Colderon, P. B., Eds.; University of Catholique de Louvain Brussels: New York, 1995; pp 11–32.
3. Braughler, J. M.; Duncan, L. A.; Chase, R. I. *J. Biol. Chem.* **1986**, *261*, 10282.
4. Braughler, J. M.; Hall, E. D. *Free Radic. Biol. Med.* **1989**, *6*, 289.
5. Hall, E. D.; Braughler, J. M. *Cent. Nerv. Syst. Trauma* **1986**, *3*, 281.
6. Kontos, H. A.; Wei, E. P. *J. Neurosurg.* **1986**, *64*, 803.
7. Oliver, C. N.; Starke-Reed, P. E.; Stadtman, E. R.; Liu, G. J.; Carney, J. M.; Floyd, R. A. *Proc. Natl. Acad. Sci. USA* **1990**, *87*, 5144.
8. Halliwell, B. *Br. J. Exp. Pathol.* **1989**, *70*, 737.
9. Ames, B. N.; Shigenaga, N. K.; Hagen, T. M. *Proc. Natl. Acad. Sci. USA* **1993**, *90*, 7915.
10. Piotrowski, J. J.; Hunter, G. C.; Eskelson, C. D.; Dubick, M. A.; Bernhard, V. M. *Life Sci.* **1990**, *46*, 715.
11. Ross, R. *Nature* **1993**, *362*, 801.
12. Braughler, J. M.; Hall, E. D. *Free Radic. Biol. Med.* **1989**, *6*, 303.
13. Panetta, J. A.; Clemens, J. A. *Ann. N.Y. Acad. Sci.* **1994**, *723*, 239.
14. Bolli, R. *Cardiovasc. Drugs Ther.* **1991**, *5*, 249.
15. Rousseau, E. J.; Davison, A. J.; Dunn, B. *Free Radic. Biol. Med.* **1992**, *13*, 407.
16. Jacobsen, E. J.; VanDoornik, F. J.; Ayer, D. E.; Belonga, R. L.; Braughler, J. M.; Hall, E. D.; Houser, D. J. *J. Med. Chem.* **1992**, *35*, 4464.
17. Grisar, J. M.; Bolkenius, F. N.; Petty, M. A.; Verue, J. *J. Med. Chem.* **1995**, *38*, 453.
18. Ohkawa, S.; Fukatsu, K.; Miki, S.; Hashimoto, T.; Sakamoto, J.; Doi, T.; Nagai, Y.; Aono, T. *J. Med. Chem.* **1997**, *40*, 559.
19. Kuehm-Caubere, C.; Caubere, B.; Caignard, D.; Bizot-Espiard, J.; Pfeiffer, B.; Cainard, D.; Guardiola-Lemaitre, B.; Renard, P. *J. Med. Chem.* **1997**, *40*, 1201.
20. Oshiro, Y.; Sarukai, Y.; Tanaka, T.; Kikuchi, T.; Hirose, T.; Tottori, K. *J. Med. Chem.* **1991**, *34*, 2014.
21. Vajragupta, O.; Toasaksiri, S.; Boonyarat, C.; Wongkrachang, Y.; Peungvicha, P.; Watanabe, H.; Boonchoong, P. *Free Radic. Res.* **2000**, *32*, 145.
22. Insight II: Apex 3D module, Molecular Simulations Inc., San Diego, CA, USA.
23. Sybyl: molecular modeling package, Tripos, St Louis, MO, USA.
24. SPSS: statistic package for windows, Chicago, IL, USA.
25. Vajragupta, O.; Pananookooln, S.; Tuntiwachwuttikul, T.; Foye, W. O. *J. Sci. Soc. Thailand* **1988**, *14*, 51.
26. Stock, J.; Gutteridge, J. M. C.; Sharp, J. R.; Dormandy, T. L. *Clin. Sci.* **1974**, *47*, 215.
27. Gutteridge, J. M. C. *Analytical Proceedings* **1990**, *27*, 219.